


Article

A Mathematical Model for Enhancing CO₂ Capture in Construction Sector Using Hydrated Lime

Natalia Vidal de la Peña^{1,*}, Séverine Marquis², Stéphane Jacques², Elise Aubry³, Grégoire Léonard¹ 
and Dominique Toye¹

¹ Department of Chemical Engineering, PEPs—Products, Environment, and Processes, Faculty of Applied Sciences, Campus Liège Sart-Tilman, University of Liège, B6a Sart-Tilman, 4000 Liège, Belgium; g.leonard@uliege.be (G.L.); dominique.toye@uliege.be (D.T.)

² Centre Pierre et Terre (CTP), Chaussée d'Antoine, 55, 7500 Tournai, Belgium; severine.marquis@ctp.be (S.M.); stephane.jacques@ctp.be (S.J.)

³ Carmeuse Coordination Center, Bd de Lauzelle 65, 1348 Louvain-la-Neuve, Belgium; elise.aubry@carmeuse.com

* Correspondence: nvidal@uliege.be

Abstract: The construction sector is among the most polluting industries globally, accounting for approximately 37.5% of the European Union's total waste generation in 2020. Therefore, it is imperative to develop strategies to enhance the sustainability of this sector. This paper proposes a multiscale COMSOL Multiphysics numerical model for an ex situ mineral carbonation process of hydrated lime. The carbonation process is characterized at both the micro- and macroscale levels, encompassing interactions within and between the particles. This model incorporates both reaction and diffusion phenomena, considering the effects of porosity and liquid-water saturation parameters. Generally, liquid-water saturation enhances the reaction kinetics but not CO₂ diffusion, while porosity improves CO₂ diffusion throughout the granular bed. The model has been experimentally validated, showing promising results by accurately characterizing carbonation tendencies and the influence of the CO₂ flow rate and the initial water-to-solid ratio on the carbonation process. The proposed mathematical model facilitates the study of various parameters, including particle radius, reactor geometry, and material porosity. This analysis is valuable for both current and future projects, as it aims to identify the most profitable configurations for the hydrated lime carbonation process.

Keywords: hydrated lime; carbonation; construction waste; CO₂ capture



Citation: Vidal de la Peña, N.; Marquis, S.; Jacques, S.; Aubry, E.; Léonard, G.; Toye, D. A Mathematical Model for Enhancing CO₂ Capture in Construction Sector Using Hydrated Lime. *Minerals* **2024**, *14*, 889. <https://doi.org/10.3390/min14090889>

Academic Editors: Fei Wang and Rafael Santos

Received: 15 July 2024

Revised: 25 August 2024

Accepted: 28 August 2024

Published: 30 August 2024



Copyright: © 2024 by the authors. Licensee MDPI, Basel, Switzerland. This article is an open access article distributed under the terms and conditions of the Creative Commons Attribution (CC BY) license (<https://creativecommons.org/licenses/by/4.0/>).

1. Introduction

The construction and demolition sectors are among the largest producers of waste, contributing approximately 37.5% of the EU's total waste generation in 2020 [1]. Construction and demolition (C&D) wastes are primarily composed of concrete, masonry, asphalt, other mineral wastes (including stone, sand, gravel, and other aggregates), wood, metal, gypsum, plastics, and miscellaneous materials. In Europe, concrete and masonry constitute between 40% and 84% of C&D wastes, while other mineral wastes account for 2% to 9% as reported in 2011 by the European Commission (DG ENV) [2]. Given the high percentage of minerals in C&D wastes, it is important to find valuable methods to reuse them. Advancing towards a circular economy by reusing these materials to produce new products or as sinks for pollutants, such as CO₂, is particularly beneficial. In the context of global greenhouse gas emissions (GHG), the construction sector contributes around 5 to 12% of the total national GHG emissions in Europe, accounting for activities from material extraction to the manufacturing of construction products and the construction and renovation of buildings [3]. In July 2024, the atmospheric CO₂ concentration was registered as 425.55 ppm (parts per million) by the monthly average Mauna Loa CO₂ report at Mauna Loa observatory [4]. Given the elevated levels of CO₂ emissions and mineral waste production, it is imperative

to develop strategies to reuse these materials and enhance the efficiency of the industry. This approach not only addresses emissions within the construction sector but can also help other industrial sectors improve their emissions profiles. By integrating CO₂ capture and reuse technologies, the overall environmental impact can be significantly reduced across multiple industries.

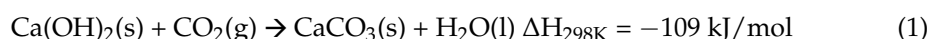
Currently, several methods have been already proposed with the aim of capturing CO₂ by using mineral materials, whether they are waste or not. These methods include aqueous wollastonite carbonation [5], the carbonation of recycled concrete aggregates [6,7], and the use of cement's storage capacity to sequester carbon dioxide [8,9], among others. As evidenced, the carbonation of mineral materials has proven to be an effective option for acting as a sink for pollutants such as carbon dioxide.

However, natural mineral carbonation faces a significant limitation, as it requires a considerable amount of time to achieve full carbonation. The natural carbonation time depends on the strength of the concrete used, which varies by country and according to specific requirements. For instance, studies have demonstrated that, in Denmark, only 4.8% of concrete was carbonated after 70 years due to the use of high-strength concrete (>35 MPa) with a low carbonation rate. Conversely, it is estimated that between 58% and 86% of concrete in Sweden and Norway will be carbonated after 100 years [10]. In contrast, other studies have indicated that complete CO₂ absorption under natural carbonation conditions of a granular bed composed of ordinary Portland cement (height of 7 cm, diameter of 7 cm, and particle size equal to 1 mm) could take between 1000 and 2000 days, while under accelerated conditions, it required approximately 10 days to achieve full carbonation [11]. Considering carbonation times during natural carbonation, it is necessary to propose faster methods and to study the influence of various parameters to optimize this process.

Mineral carbonation can be performed in two main ways, namely *in situ* and *ex situ*. *In situ* carbonation involves the direct injection of carbon dioxide into geological formations containing magnesium and calcium-based minerals, which then form carbonates [12]. *Ex situ* carbonation, on the other hand, occurs in an industrial process where the carbonatable components within the mineral material react with CO₂ either directly in a single phase or indirectly in several stages, involving the dissolution of minerals before carbonation [12].

Considering that lime products and derivatives are used in numerous applications (as building materials, in the production of pozzolans used as additives, and as lubricants in steel manufacturing), their presence in mineral construction waste is highly probable [13]. Studies have shown that lime-based materials could capture between 23.50 and 49.81 Mt C per year [14]. Specifically focusing on hydrated lime, Erans, M et al. demonstrated that 78% carbonation was achieved after 740 h of exposure, with no further changes observed beyond this period [15]. In this study, hydrated lime was selected as the material for investigation due to its potential to capture CO₂. Another reason is that it is a key material for the partners of the Mineral Loop project, funded by the Walloon region and involving several industrial partners, including a lime producer [16].

Hydrated lime, depending on its intended use, requires careful consideration of its carbonation with CO₂ from the air. To effectively control and analyze the CO₂-capture process, it is crucial to isolate hydrated lime to prevent premature carbonation, which could compromise the study. The simplified carbonation reaction of hydrated lime with carbon dioxide is represented as follows [17]:



In this paper, the proposal is to model the carbonation process of hydrated lime as expressed in Equation (1) as a way to capture carbon dioxide. Despite the carbonation reaction of hydrated lime appearing to be simple, it is actually quite complex, due to the multitude of phenomena that occur during the process. Among these complexities, the chemical reaction itself is not straightforward and requires precise control of environmental conditions, such as relative humidity, temperature, and pressure [11,12]. Additionally, the

kinetics of carbonation are not well-studied and need to be thoroughly understood. On the other hand, water is required at the start of the process to dissolve the mineral and initiate the chemical reaction. The overall carbonation reaction described in Equation (1) involves the following dissolution steps: (i) $\text{Ca}(\text{OH})_2$ dissolves with the water located in the pores, leading to the dissociation of Ca^{2+} and OH^- ions; (ii) gaseous CO_2 dissolves into the alkaline pore solution, forming a hydrated aqueous phase; (iii) CO_2 subsequently reacts with OH^- ions to form carbonic acid (H_2CO_3), which rapidly dissociates into bicarbonate (HCO_3^-) and carbonate CO_3^{2-} ions; and, finally, (iv) Ca^{2+} ions react with carbonate ions to precipitate calcium carbonate [17–21].

Regarding the reaction specified in Equation (1), during carbonation, water is produced, leading to an increase in the liquid-water saturation within the system. This water production can lead to fully saturated conditions, potentially filling the porosity and limiting CO_2 diffusion to the reaction site [18,19]. At this point, it is thus observed that water plays a crucial role in the carbonation process.

Furthermore, a dual-scale model is essential due to the presence of two scales of porosity, namely one within the hydrated lime particles and another between them [11]. CO_2 must diffuse through both porosities, which evolve over time as the $\text{Ca}(\text{OH})_2$ converts to CaCO_3 [11,22,23]. The production of calcium carbonate leads to an increase in the solid volume, causing the structure of the reacting medium to evolve throughout the reaction and adding further complexity to the process [24].

Taking all these elements into account, this paper proposes a mathematical model to predict and understand the behavior of a model material (pure hydrated lime) for CO_2 capture under simplified conditions (isobaric and isothermal). Through detailed model explanations, various phenomena are elucidated and characterized. The influences of different parameters on the system, such as porosity and liquid-water saturation, are thoroughly examined. Ultimately, the model is validated using the experimental results of total carbon captured from the lab-scale setup, and conclusions drawn from these results are discussed.

In conclusion, the primary objective of this paper is to propose a validated model that accurately represents the phenomena present in the carbonation process and can subsequently be extended first to non-isothermal conditions and, then, to more complex materials and capture setups.

2. Materials and Methods

2.1. Experimental Work

A series of carbonation experiments were conducted using pure hydrated lime to investigate the material's behavior during the carbonation process. The primary objective of these experiments was to generate experimental data that could elucidate the impact of various parameters on the carbonation process. Specifically, the study focused on analyzing how the initial water-to-solid ratio and the flow rate of CO_2 influence the carbonation performance. The experimental results obtained from these tests are later used to validate the mathematical model proposed in this article.

2.1.1. Material Characteristics and Experimental Procedure

The carbonation experiments were conducted using pure hydrated lime, a fine powder with an initial particle diameter of 35.5 μm . Before starting the carbonation process, the hydrated lime was dried overnight in a standard oven at 200 °C to eliminate any moisture and achieve zero relative humidity. This step is crucial to prevent the hydrated lime from prematurely reacting with the CO_2 in the air before the carbonation process begins.

After drying, a portion of the sample was subjected to two key measurements, namely mercury intrusion porosimetry (MIP) and total carbon analysis. MIP is a widely utilized technique for measuring the porosity and pore size distribution of porous materials. In this study, the MIP test was performed using a Quantachrome Poremaster 60 (CARPOR-University of Liège, Liège, Belgium), operating within a pressure range of 0.01

to 400 MPa [25]. In parallel, a total carbon analysis was conducted using a CS744 carbon/sulfur analyzer (Centre Terre et Pierre company, Tournai, Belgium). For this analysis, 500 mg of dried sample were introduced into the analyzer and combusted in a stream of oxygen using radio-frequency induction heating. During combustion, the carbon in the sample oxidizes to form CO_2 , which is then measured using a non-dispersive infrared (NDIR) cell to determine the total carbon content [26]. The initial tests revealed a bed porosity of 0.65 and a particle porosity of 0.1. The total carbon content was found to be 0.21%.

Following the drying process, 100 g of hydrated lime were mixed with the required amount of water. The mixture was manually stirred and then left to homogenize for two hours in a closed bag to prevent any early carbonation reactions. After this rest period, the mixture was well-homogenized and ready for the carbonation process.

Afterward, seventy grams of the prepared material were introduced into an aluminum cup with the following dimensions: a base diameter of 70 mm, a top diameter of 83 mm, and a height of 25 mm. This cup was then placed into a reactor with a capacity of 1.4 L. The reactor was equipped with two holes at the top, one for the entry of carbon dioxide and another for its exit (see Figure 1a). Once the cup was properly positioned inside the reactor, pure carbon dioxide was introduced through the inlet hole located on the right side of Figure 1a. The CO_2 flowed through the reactor for the specific carbonation period. Upon completing the carbonation process, the semi-conical aluminum cup was transferred to a dryer for at least 12 h. This step ensured the removal of any residual moisture from newly carbonated material before analyzing its carbon content in the laboratory. Following the drying process, mercury intrusion porosimetry (MIP) and total carbon tests were conducted.

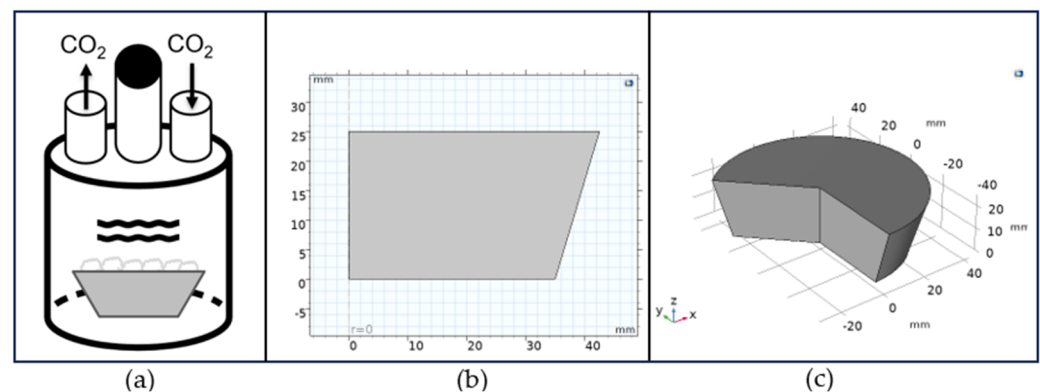


Figure 1. (a) Scheme of the experimental setup. (b) Adaptation of the coup geometry into a 2D axisymmetric COMSOL Multiphysics 6.2 model. (c) Adaptation of the coup geometry into a 3D COMSOL Multiphysics 6.2 model.

2.1.2. Experiments Conducted to Validate the Proposed Mathematical Approach

To validate the proposed mathematical model, a series of experiments were conducted. For the carbonation experiments, 100 g of pure calcium hydroxide were weighed and mixed with the proportional amount of water needed for each experiment. Table 1 presents the mass ratio between the mass of water added before carbonation and the initial mass of calcium hydroxide (w_s), along with the CO_2 flow rate and the carbonation time for each experiment conducted.

Table 1. Conditions of the carbonation experiments: w_s (g/g) as the mass ratio between the mass of the water added before carbonation and the initial mass of calcium hydroxide, the CO_2 flow rate introduced, and the carbonation time.

Carbonation Experiment	w_s (g/g)	CO_2 Flow Rate ($\text{mL}\cdot\text{min}^{-1}$)	Carbonation Time (min)
1	0.1	100	30
2	0.1	100	45
3	0.2	100	30
4	0.2	100	45
5	0.4	100	30
6	0.4	100	45
7	0.1	200	30
8	0.1	200	45
9	0.2	200	30
10	0.2	200	45
11	0.4	200	30
12	0.4	200	45

2.2. Modelling Work: Dual Scale Approach

The model proposed in this article considers the hydrated lime as a powdered material composed of spherical particles, which are stacked to form a granular bed and arranged regularly. The concentration of the granular bed is calculated using the mass of calcium hydroxide measured during the experiments, the volume of the granular bed, and the molar mass of $\text{Ca}(\text{OH})_2$. Furthermore, the concentration of carbon dioxide above the granular bed is maintained at a constant value once the reactor is completely filled with CO_2 , with the CO_2 introduced in its pure form. This condition, along with the specific geometry of the bed, is modeled using the software COMSOL Multiphysics 6.2 as a 2D axisymmetric system.

In this system, two scales are considered, namely the microscale, corresponding to individual particles, and the macroscale, relating to the granular bed as a group of these particles. The granular bed is modeled as a truncated cone, as depicted in Figures 1b and 2, with a height of 25 mm, a base diameter of 70 mm, and a top diameter of 85 mm. The bed has a porosity of 0.65, while the particles within the granular bed, composed of pure calcium hydroxide, have a porosity of 0.1 and a diameter of $35.5\ \mu\text{m}$. As a first approach, the system is assumed to be isothermal and isobaric, maintained at 298 K and 1 bar. This dual-scale approach recognizes that different phenomena manifest differently at each scale. First, the role of water in the carbonation reaction will be described. Then, the impact of carbonation on porosity will be presented and, finally, the role of diffusion.

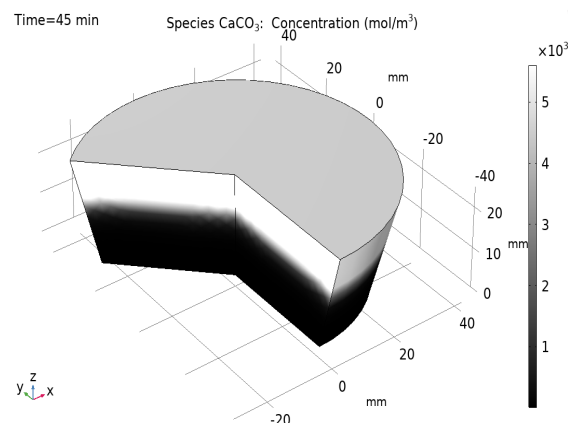


Figure 2. CaCO_3 concentration along the reactor after 45 min of carbonation.

2.2.1. Role of Water in the Carbonation Reaction

During carbonation, water also plays a crucial role, both as a product and as a necessary component for initiating the chemical reaction. To facilitate the carbonation reaction expressed by Equation (1) and to allow the reaction to occur, it is necessary to humidify the material. This aids in the dissolution of Ca^{2+} and OH^- ions, the dissolution of CO_2 from the gas phase into the aqueous phase, and the subsequent reaction between these species to form CaCO_3 [11,12,21].

In the proposed mathematical model, the primary focus is on the simplified reaction between calcium hydroxide and carbon dioxide, as shown in Equation (1). The dissolution steps (i–iv) are not explicitly modeled, since they are considered to occur rapidly due to the limited amount of water in the material [11]. Instead, the presence of water is represented by the initial water-to-solid ratio (w_s), quantified as the mass of water initially added in relation to the initial mass of solid material, and the liquid-water saturation parameters inside the particle (S_p) and between the particles (S_b). The liquid-water saturation of the bed represents the degree to which the spaces between particles are filled with water, and the liquid-water saturation of the particles represents the degree to which the pores within the individual particles are filled with water.

Liquid-water saturation (S_i) is calculated based on the water concentration, the porosity, and the water density. The calculation for liquid-water saturation at both scales is given by Equation (2), where i can be b for the granular bed scale and p for the particle scale [18].

$$S_i = \frac{[w]_i (\text{mol}/\text{m}^3) \cdot M_{\text{H}_2\text{O}} (\text{kg}/\text{mol})}{\rho_w (\text{kg}/\text{m}^3) \cdot \phi_i} \quad (2)$$

As explained before, the presence of liquid water positively influences the kinetics of the carbonation reaction. The reaction rate is assumed to be extremely fast in comparison with the diffusion phenomena [11]. Considering that the kinetics of the reaction have been simplified, it follows the behavior of a second-order reaction. The kinetic rate, denoted as r ($\text{mol} \cdot \text{mol}^{-3} \cdot \text{s}^{-1}$), is expressed as follows.

$$r = k \cdot [\text{CO}_2] \cdot [\text{Ca}(\text{OH})_2] \quad (3)$$

where k is the kinetic constant ($\text{m}^3 \cdot (\text{mol} \cdot \text{s})^{-1}$), and $[\text{CO}_2]$ and $[\text{Ca}(\text{OH})_2]$ correspond to the concentration of carbon dioxide and calcium carbonate ($\text{mol} \cdot \text{m}^{-3}$), respectively. The kinetic constant value is obtained by the next equation as a function of liquid-water saturation.

$$k = k_0 \cdot \frac{S_i}{0.79} \quad (4)$$

where k_0 is a base kinetic constant, equal to $0.0025 \text{ m}^3 \cdot (\text{mol} \cdot \text{s})^{-1}$ [17,27]. However, even though this parameter has a positive influence on the kinetics of the reaction, there are limits that must be considered regarding the liquid-water saturation parameter. The first one is the initial water requirement. If there is no initial water, the reaction cannot proceed because S_i will be zero, effectively nullifying the kinetics in Equation (4). The second one is the full saturation limit. When the liquid-water saturation approaches 1, the material porosity becomes fully flooded. The kinetic rate reaches its maximal value, but the reaction is nevertheless slowed down due to diffusional limitations, as will be detailed in Section 2.2.3.

2.2.2. The Role of Porosity in CO_2 Diffusion and Carbonation of Hydrated Lime

During the carbonation of calcium hydroxide, the calcium carbonate forms within the micropores, blocking the porosity of the particles and inhibiting the original porosity that was present [20,28]. As carbonation proceeds, it is experimentally observed that the particle's internal porosity (ϕ_p) becomes almost instantaneously unavailable. This means that, once the carbonation process begins, ϕ_p is effectively reduced to zero for times greater than zero, indicating that the internal pores of the particles are filled or blocked by the

reaction products. To validate this assumption, a mercury intrusion porosimetry (MIP) test was conducted. Upon analyzing the material, it was confirmed that the microporosity decreased from 0.1 to 0.0 after 45 min of carbonation, utilizing an initial water-to-solid ratio of 0.2 and a CO₂ flow rate of 200 mL·min⁻¹ at 298 K and atmospheric pressure.

Carbonation not only reduces microporosity but also leads to an increase in the solid volume due to the formation of calcium carbonate. This volume increase can be calculated based on the densities and molar masses of the reactants and products. The density of CaCO₃ is 2.74 kg·cm⁻³ (ρ_{CaCO_3}), and its molar mass is 100.09 g·mol⁻¹ (M_{CaCO_3}). Meanwhile, the density of Ca(OH)₂ is 2.21 kg·cm⁻³ ($\rho_{\text{Ca(OH)}_2}$), and its molar mass is 74.09 g·mol⁻¹ ($M_{\text{Ca(OH)}_2}$).

By calculating the molar volume of one mole of each component, it is found that the molar volume of CaCO₃ is approximately 4 cm³·mol⁻¹ greater than that of Ca(OH)₂. This can be represented by the following equations:

$$\frac{M_{\text{Ca(OH)}_2}}{\rho_{\text{Ca(OH)}_2}} < \frac{M_{\text{CaCO}_3}}{\rho_{\text{CaCO}_3}} \quad (5)$$

$$V_m^{\text{Ca(OH)}_2} < V_m^{\text{CaCO}_3} \quad (6)$$

Considering that microporosity is rapidly blocked by the formation of calcium carbonate and that macroporosity increases due to the expansion of the solid bed volume, an overall increase in intergranular porosity, or bed porosity, on the macroscale is developed [29]. The model accounts for the increase in bed porosity over time by considering the volume increase associated with the production of one mole of calcium carbonate. The increase in bed porosity is defined by the following equation:

$$\phi_b = \phi_b^0 + \Delta\bar{V} \left(\frac{\text{m}^3}{\text{mol}} \right) \cdot [\text{CaCO}_3] \left(\frac{\text{mol}}{\text{m}^3} \right) \quad (7)$$

where ϕ_b^0 is the initial bed porosity, $\Delta\bar{V}$ is the volume difference between one mole of calcium carbonate and one mole of calcium hydroxide, and $[\text{CaCO}_3]$ is the concentration of calcium carbonate during the carbonation process. By incorporating these dynamics, the model provides a comprehensive understanding of how carbonation influences both microporosity and macroporosity, enhancing the predictive accuracy for CO₂-capture efficiency for construction and mineral materials. After conducting the MIP test, it was observed that the bed porosity increased from 0.65 to 0.71 after 45 min of carbonation when using an initial water-to-solid ratio of 0.2 and a flow rate of 200 mL·min⁻¹.

2.2.3. The Role of Diffusion

Diffusion describes how CO₂ enters and spreads inside and between the particles along the granular bed [30,31]. In this system, CO₂ transport occurs via diffusion between the particles (no convection) and within the particles [11,30]. In the carbonation of mineral materials, diffusion is influenced by two principal parameters, as explained before, namely by porosity and liquid-water saturation. These parameters play a crucial role in the carbonation process of hydrated lime, influencing the way CO₂ diffuses through the material and reacts to form carbonates. The relationship between porosity, liquid-water saturation, and the diffusion coefficient of CO₂ in the granular bed is based on the saturation-dependent model proposed by Millington and Quirk (1961) [32–34]. This model characterizes the diffusion coefficient of a fluid by incorporating a constant specific diffusion coefficient ($D_{\text{CO}_2}^0$) influenced by a resistance factor (F_b) [11].

$$D_b^{\text{CO}_2} = D_{\text{CO}_2}^0 \cdot F_b \quad (8)$$

where $D_{CO_2}^0$ is the specific diffusion coefficient of CO_2 outside the porous medium, with a value equal to $1.6 \times 10^{-5} \text{ m}^2 \cdot \text{s}^{-1}$ at 298 K and a pressure of 1 bar. F_b is a resistance factor that accounts for the tortuosity effects and the reduction in space available for gas diffusion in a partially saturated porous medium. According to the model proposed by Millington and Quirk (1961) and the mathematical model proposed by Thiery et al. the parameter F_b is described as follows [11,32–34].

$$F_b = \phi_b^{4/3} \cdot (1 - S_b)^{10/3} \quad (9)$$

where ϕ_b corresponds to the bed porosity and S_b to the liquid-water saturation of the bed. On the other hand, to describe the diffusion of CO_2 inside the particles, a similar equation is used.

$$D_p^{CO_2} = D_{CO_2}^0 \cdot \phi_p^{2.7} \cdot (1 - S_p)^{4.2} \quad (10)$$

where ϕ_p is the porosity of the particles, and S_p is the liquid-water saturation inside the particles [11]. On the other hand, focusing on the diffusion of the water, it is necessary to characterize it in both the bed and inside the particles. The equations used to characterize the water diffusion are the same ones as for the CO_2 but consider the standard diffusion coefficient of water at 25 °C. The equations for water diffusion are the following ones.

$$D_b^{H_2O} = D_{H_2O}^0 \cdot \phi_b^{4/3} \cdot (1 - S_b)^{10/3} \quad (11)$$

$$D_p^{H_2O} = D_{H_2O}^0 \cdot \phi_p^{2.7} \cdot (1 - S_p)^{4.2} \quad (12)$$

where $D_{H_2O}^0$ is the standard diffusion coefficient of water at 298 K equal to $2.3 \times 10^{-9} \text{ m}^2 \cdot \text{s}^{-1}$ [35]. To complete the diffusion coefficients list to be used in the model, those of the solid components, $Ca(OH)_2$, and $CaCO_3$ are fixed to arbitrarily low values ($1 \times 10^{-12} \text{ m}^2 \cdot \text{s}$) to account for the fact that they remain static during the carbonation process.

2.2.4. Computational Modeling: Operational Conditions and Assumptions

Although the experimental setup consists of the large reactor and the aluminum cup, the initial modeling in COMSOL Multiphysics focuses solely on the cup's geometry. The modeling process involves two stages, namely the 2D axisymmetric model and the 3D cup model. Initially, the geometry of the cup is modeled in 2D as an axisymmetric system (Figure 1b) to simplify the computational process, while capturing the essential characteristics of the system. Then, the model is expanded to a full 3D representation of the cup (see Figure 1c), allowing for more accurate simulations and predictions of the carbonation process.

The operational conditions for the system are determined based on its behavior under specific constraints and are summarized as follows:

- Initially, the concentration of carbon dioxide above the cup is assumed to be zero, given that the reactor contains only air. Subsequently, as the reactor is supplied with pure CO_2 , the concentration of CO_2 increases progressively until it reaches a steady-state value above the cup;
- The water concentration at the top of the cup is assumed to be zero. This assumption is based on the outgoing gas carrying away any surface water, thereby preventing any water accumulation in the cup. This scenario is feasible because the flow rate of the gas is high and dry, ensuring excellent mass transfer at the surface. Additionally, the sweeping efficiency of the gas flow is sufficient to maintain the liquid-water saturation at the top of the reactor at a very low value;
- Due to the presence of the aluminum wall, there is no flux through the sides or bottom of the cup;
- The pressure is maintained constant at 1 bar and, in the first step, the temperature is considered as constant at 298 K.

3. Results

Following the implementation of the model in COMSOL Multiphysics 6.2, the results pertaining to the carbonation process are presented in the subsequent subsections. First, the results concerning the production of CaCO_3 are presented, as well as the evolution of the diffusion coefficient of CO_2 and the carbonation rate during the carbonation process. This is followed by the validation of the mathematical model against the experimental data. Finally, a sensitivity analysis is shown to study the influence of the initial water-to-solid ratio and the initial bed porosity on the carbonation process.

3.1. Calcium Carbonate Production and Carbon Dioxide Diffusion during the Carbonation Process

In this subsection, the results correspond to the actual properties of the carbonated samples, namely an initial concentration of pure calcium hydroxide of $4659.8 \text{ mol}\cdot\text{m}^{-3}$, an initial particle porosity of 0.1, an initial bed porosity of 0.65, a particle diameter equal to $35.5 \text{ }\mu\text{m}$, and an initial water-to-solid ratio equal to 0.1. The CO_2 is maintained at $200 \text{ mL}\cdot\text{min}^{-1}$. In the following representations of the granular bed, the value of the x-axis equal to 0 mm represents the bottom of the granular bed, and when its value is equal to 25 mm, it refers to the top of it.

As the main objective of this process is the production of calcium carbonate, Figure 2 shows the production of CaCO_3 within the 3D granular bed from top to bottom after 45 min of carbonation. It is observed that, after this duration, the granular bed is almost half carbonated. A carbonation front is clearly observed along the granular bed.

Furthermore, Figure 3 illustrates two key aspects. Figure 3a shows the variation in the diffusion coefficient throughout the process, while Figure 3b depicts the variation in the carbonation rate during the carbonation process. Regarding Figure 3a, it is notable that, during the first five minutes of carbonation, the diffusion coefficient increases sharply. As the diffusion coefficient is related to the porosity and the liquid saturation, this behavior indicates that, at this stage, the increase in the bed porosity related to the conversion of $\text{Ca}(\text{OH})_2$ to CaCO_3 has a greater influence than the porosity decrease, due to pore filling by the water generated during the process. However, between 5 and 15 min of carbonation, the diffusion coefficient significantly decreases, implying that, during this period, the influence of the water outweighs the benefits of increased porosity.

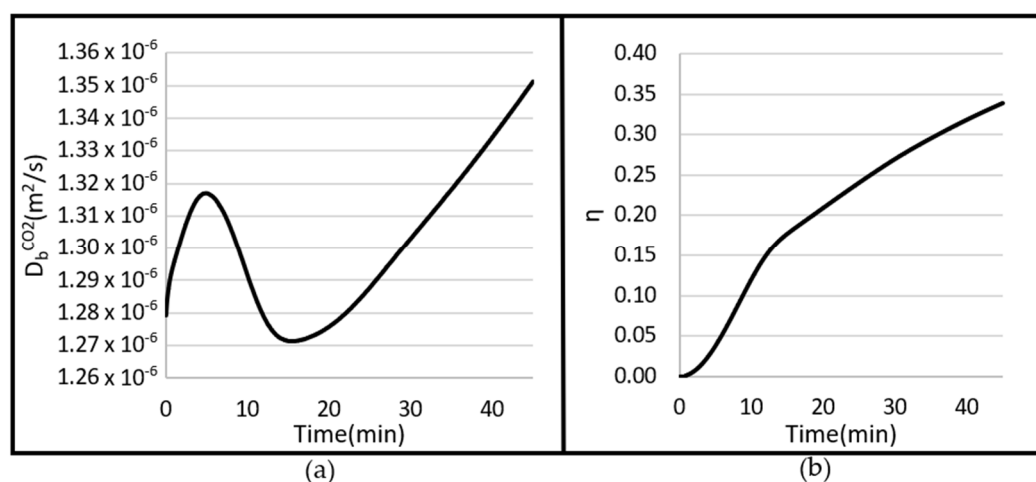


Figure 3. (a) Average evolution of the diffusion coefficient with the carbonation time over the whole solid bed. (b) Volumetric average carbonation rate variation during the carbonation process.

This observation is corroborated by Figure 3b, which shows the volumetric average carbonation rate during the carbonation process. In the model, the carbonation rate (η) measures the concentration of calcium carbonate produced in relation to the maximum amount that could be produced, and it is calculated as follows.

$$\eta = \frac{[CaCO_3] \left(\frac{\text{mol}}{\text{m}^3} \right) - [CaCO_3]_{t=0} \left(\frac{\text{mol}}{\text{m}^3} \right)}{[Ca(OH)_2]_{t=0} \left(\frac{\text{mol}}{\text{m}^3} \right)} \quad (13)$$

where $[CaCO_3]_{t=0}$ (mol/m³) refers to the initial concentration of calcium carbonate if the sample is initially carbonated, $[CaCO_3]$ (mol/m³) is the concentration of calcium carbonate during the process, and $[Ca(OH)_2]_{t=0}$ (mol/m³) is the initial concentration of calcium hydroxide, i.e., the maximum molar concentration of calcium carbonate that could be produced.

Regarding Figure 3b, a steeper increase in the carbonation rate is observed between 5 and 15 min of carbonation. This reveals a rapid reaction between the hydrated lime and CO₂, resulting in substantial water production and a higher liquid-water saturation in a shorter time, thus explaining the decrease in the diffusion coefficient. Finally, regarding Figure 3a,b, after 15 min, both the diffusion coefficient and the carbonation rate increase with time, but at a much slower rate as compared to the beginning of the process. Additionally, the proposed process shows that the bed porosity increases from 0.65 to 0.68 after 45 min of carbonation.

3.2. Model Validation

To validate the mathematical model, the total carbon weight percentage after carbonation (TC) is measured experimentally using a total carbon analysis. The total carbon parameter from the simulation results is calculated using the next equation.

$$TC = \frac{\eta * M_C \left(\frac{\text{g}}{\text{mol}} \right)}{\left(\eta * M_{CaCO_3} \left(\frac{\text{g}}{\text{mol}} \right) + (1 - \eta) * M_{Ca(OH)_2} \left(\frac{\text{g}}{\text{mol}} \right) \right)} \quad (14)$$

M_C is the molar mass of carbon, and it is equal to 12 (g/mol). M_{CaCO_3} is the molar mass of calcium carbonate with a value of 100 (g/mol), and $M_{Ca(OH)_2}$ is the molar mass of calcium hydroxide and is equal to 74 (g/mol). In this case, the material has an initial total carbon content that is experimentally measured to 0.21% by a total carbon test.

The total carbon value provided by the model is based on a volumetric average calculation, which is important to mention because carbonation occurs from the top to the bottom of the cup, inducing vertical concentration profiles. Volume averaging allows for flattening of the profile. This approach is required because experimental samples for carbon measurement are not taken at specific points in the bed. They are sampled as randomly as possible. So, comparing on the basis of the volumetric average appears more accurate and representative of the overall carbonation process.

To compare and analyze the results obtained experimentally with the model, Figure 4 is provided. Regarding Figure 4a showing results after 30 min, it has been observed experimentally that a higher initial water-to-solid ratio results in greater total carbon. However, looking at Figure 4b, after 45 min of carbonation, the difference in total carbon between the initial water-to-solid ratios of 0.2 and 0.4 is less pronounced. This indicates that, after 45 min of carbonation, the system starts to become saturated in a similar way for both initial water-to-solid ratios of 0.2 and 0.4.

On the other hand, regarding Figure 4, the CO₂ flow rate significantly influences the carbonation process. Higher flow rates (200 mL·min⁻¹, represented in blue) yield much higher total carbon values compared to lower flow rates (100 mL·min⁻¹, represented in orange). As the nature of the gas does not change (pure CO₂), this suggests that increasing the flow rate allows for a faster flushing of the air initially present in the reactor, so that the carbonation is more efficient in the given timeframe.

Furthermore, Figure 4a,b presents a comparison between the total carbon achieved as predicted by the model (dotted bars) and the experimental results (plain bars). In general, the model is considered successfully validated due to the good agreement with the experimental results. However, there is an underestimation of the carbonation at high

initial water-to-solid ratios, especially at high gas flow rates. This can perhaps be attributed to the isothermal assumption in the model, which neglects the evaporation of water during carbonation. The exothermic nature of the carbonation reaction generates heat, leading to increased temperatures and causing water to evaporate. This dynamic is not fully captured yet by the model, which assumes that water evaporation is limited to the superficial layer removed by the passing gas.

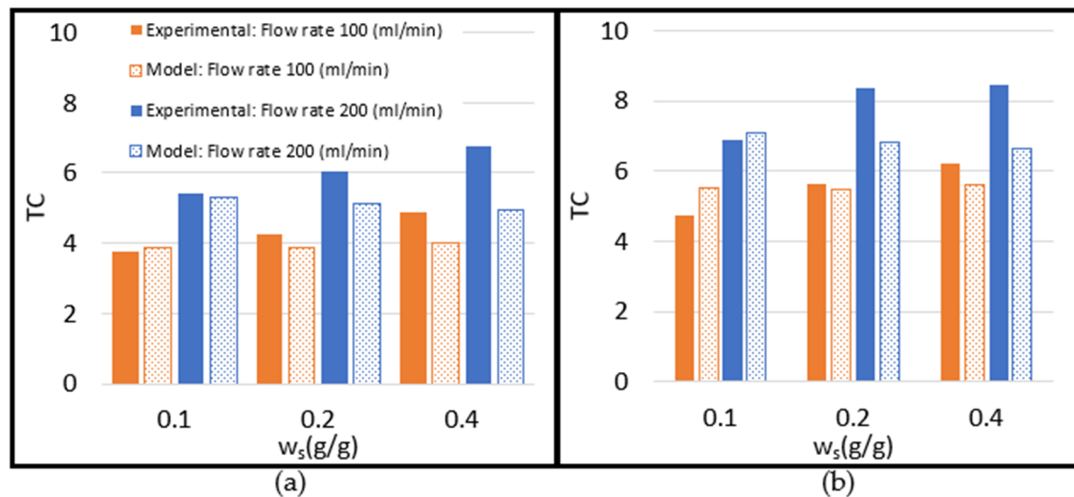


Figure 4. (a) Total carbon results of the experiments after 30 min of carbonation. (b) Total carbon results of the experiments after 45 min of carbonation.

In order to deeply analyze the accuracy of the model, three error metrics were investigated. First, the relative errors for each individual experiment were examined. Subsequently, the mean absolute percentage error (MAPE) was calculated to assess the accuracy of the model by determining the average absolute percentage difference between the predicted values and the actual experimental values. Additionally, the root mean square error (RMSE) was evaluated, which quantifies the model’s performance by measuring the square root of the average squared differences between the predicted and actual values. The MAPE and RMSE analyses were conducted on grouped data, specifically as a function of the initial water-to-solid ratios used in the experiments. This approach allowed for a more detailed assessment of the model’s performance across different experimental conditions.

Table 2 presents the results of the experiments conducted to validate the model. The table lists the experimental conditions, followed by the total carbon measured experimentally, the carbonation rate, the total carbon projected by the model, the relative error, the MAPE error, and the RMSE error.

Table 2. Comparison of experimental and simulated total carbon results.

Carbonation Experiment	ws (g/g)	CO ₂ Flow Rate (mL/min)	Carbonation Time (min)	Experimental TC (wt.%)	Simulated η (%)	Simulated TC (wt.%)	Relative Error (%)	MAPE (%)	RMSE
1	0.10	100	30	3.76	30.89	3.89	3.46		
2	0.10	100	45	4.76	44.61	5.52	15.97	2	0.42
3	0.10	200	30	4.26	31.15	3.89	8.69		
4	0.10	200	45	5.66	44.33	5.46	3.53		
5	0.20	100	30	4.88	32.44	4.02	17.63		
6	0.20	100	45	6.24	45.70	5.61	10.10	12	0.93
7	0.20	200	30	5.43	42.69	5.29	2.58		
8	0.20	200	45	6.88	57.70	7.09	3.05		
9	0.40	100	30	6.08	41.41	5.11	15.95		
10	0.40	100	45	8.35	55.60	6.81	18.44	19	1.42
11	0.40	200	30	6.76	40.15	4.93	27.07		
12	0.40	200	45	8.53	54.48	6.65	21.49		

Regarding Table 2, it is observed that the relative errors range from 3% to 27%. Figure 5 summarizes the relative errors presented in Table 2, providing a visual representation of the model's accuracy. As shown in Figure 5, nearly all data points simulated by the proposed model fall within a margin of error of $\pm 20\%$ compared to the experimental results. This indicates that the carbonation process described by the model is physically sound. The two yellow points in Figure 5, out of the range, correspond to the experiments conducted with a flow rate of $200 \text{ mL}\cdot\text{min}^{-1}$ and an initial water-to-solid ratio of 0.4 after 30 and 45 min of carbonation. Overall, almost all relative errors are below 20%, which aligns with the accuracy goal established by the Mineral Loop project. However, because these calculations involve relatively small numbers (with a maximum total carbon value of 12), the relative errors alone do not provide substantial insight into the model's accuracy. This limitation is why the MAPE and RMSE analyses were conducted as well.

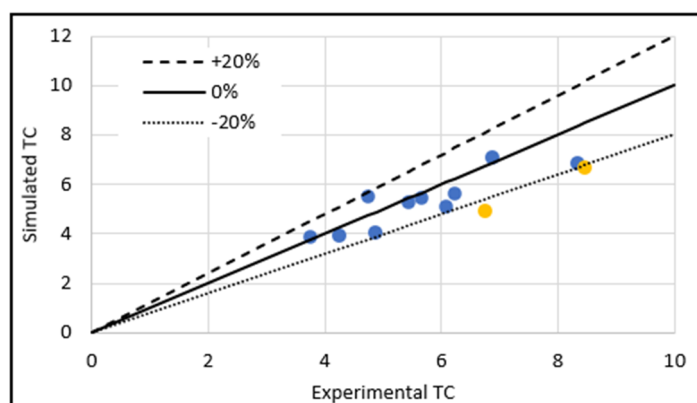


Figure 5. Model validation representation of the point inside and outside the margin of $\pm 20\%$ error.

Focusing on the MAPE error, it is noteworthy that, when the water-to-solid ratio is 0.1, the error is just 2%, which supports the conclusion that the model is accurate at low water-to-solid ratios. Extending the analysis to experiments with an initial water-to-solid ratio of 0.2, the MAPE error is 12%, which indicates a slight decrease in accuracy compared to the 0.1 ratio, while the water-to-solid ratio is still relatively low. Furthermore, at higher water-to-solid ratios, the MAPE error increases significantly, reaching nearly 20%.

Similarly, the RMSE analysis reveals a consistent trend. At low water-to-solid ratios, the model predicts values that deviate by less than one from the actual experimental results. In contrast, at higher water-to-solid ratios, the model's predictions can deviate by as much as 1.42 from the actual values.

In summary, Table 2 indicates that the model presented in this study is accurate when applied to low water-to-solid ratios ($w_s = 0.1$ or 0.2) but shows decreased accuracy at higher ratios ($w_s = 0.4$). As already shown and explained in Figure 4, this discrepancy is believed to be due to temperature increase during the carbonation process. The model is simplified by assuming an isothermal process, but in reality, the reaction is exothermic. As the temperature rises, water begins to evaporate, creating voids that allow CO_2 to enter, thus enhancing carbonation. When the initial water-to-solid ratios are 0.1 or 0.2, the temperature increase is not as pronounced, as it is with higher water-to-solid ratios. During the experiments, condensed water was observed on the walls of the reactor, supporting the conclusion that evaporation occurs in practice. Moreover, the amount of condensed water was visually greater in the experiments with a water-to-solid ratio of 0.4 than in those with ratios of 0.1 or 0.2, further confirming the reduced accuracy of the model at higher water-to-solid ratios due to the evaporation phenomenon.

3.3. Influence of Initial Water-to-Solid Ratio and Initial Bed Porosity in Carbonation Process

The aim of this model is to identify the optimal values of the controlled parameters to maximize the profitability of the mineral carbonation process. To demonstrate the model's

effectiveness at finding these optimal values, a sensitivity analysis has been conducted by introducing different initial water-to-solid ratios and initial bed porosities. The groups of parameters chosen have been adapted to our material from those proposed by Thiery et al. [11] and are summarized in Table 3.

Table 3. Parameters used to perform the sensitivity analysis of the influence of the initial bed porosity, ϕ_b^0 , and the initial water-to-solid ratio, w_s (g/g).

Particle Diameter (μm)	CO ₂ Flow Rate (mL/min)	ϕ_b^0	w_s (g/g)
35.5	200	0.3	0.35
35.5	200	0.41	0.45
35.5	200	0.49	0.55
35.5	200	0.54	0.6
35.5	200	0.61	0.8

Figure 6 shows the simulated results of the carbonation rate for the selected values of parameters. It allows for performing a sensitivity analysis. Figure 6a depicts the variation of the carbonation rate along the granular bed after 45 min of carbonation. The point $x = 25$ mm represents the top of the cup and $x = 0$ mm the bottom. In this figure, the first notable observation is the clear carbonation front along the granular bed. In this case, after 45 min of carbonation, in all the configurations, the carbonation front has advanced between 5 and 7 mm from the top to the bottom of the cup. It is observed that, when the initial bed porosity is 0.54 and the initial water-to-solid ratio is 0.6, the front advances faster than in all other cases.

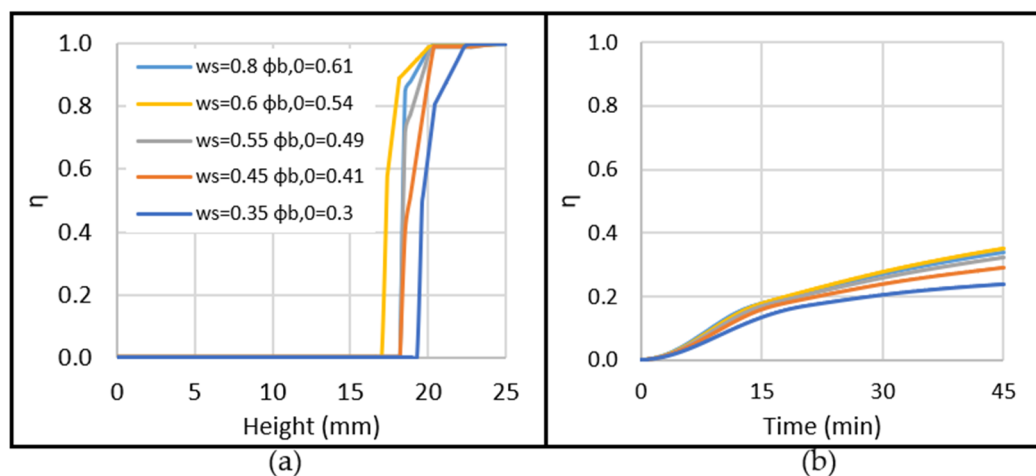


Figure 6. (a) Carbonation rate variation along the granular bed after 45 min of carbonation. (b) Volumetric average carbonation rate variation during the carbonation process for different values of initial water-to-solid ratios and initial bed porosities.

Furthermore, Figure 6b represents the volumetric average carbonation rate of the granular bed as a function of time. What is interesting about this figure is that, considering these configurations, the volumetric average carbonation rate initially increases rapidly, up to 0.2 in 15 min, and then more slowly, up to 0.4 between 15 and 45 min of carbonation. This indicates that, after 45 min, the carbonation process is slower, which is logical given that the carbonation front has not yet advanced to the midpoint of the granular bed. From Figure 6a,b, it is evident that, for the material under study, the optimal configuration for the group of parameters considered, which are listed in Table 2, is an initial water-to-solid ratio of 0.6 and an initial bed porosity of 0.54. This indicates that high values of initial water-to-solid ratios or porosities are not beneficial for the system, nor are low values. When the initial water-to-solid ratio is higher than the optimal value, calcium hydroxide clusters form, impeding the penetration of carbon dioxide into the material and reducing

the rate of carbonation [36]. Conversely, when the initial water-to-solid ratio is lower than the optimal value, the solubilization of calcium and hydroxide ions is too low and insufficient, preventing the reaction from occurring [11,12,18].

It is important to note that the optimal water-to-solid ratio varies depending on the system under study. For instance, in the study conducted by Thiery et al., which focused on cement-based materials, the optimal carbonation rate was observed with an initial water-to-solid ratio of 0.45, instead of 0.6 in our case [11].

4. Discussion

The developed mathematical model offers a detailed characterization of chemical reactions and diffusion phenomena, making it a valuable tool for understanding and scaling up the carbonation process. It has been observed that the diffusion phenomena depend on the stage of carbonation, showing higher values of the diffusion coefficient at the start of carbonation, lower values when a large amount of calcium carbonate and water are produced in a short time, and then a linear increase once the rapid production phase is over. In this case, it has been shown that, when using calcium hydroxide, this rapid production period lasts for approximately 5 min. The conclusion drawn from this phenomenon is that, during the initial stages of carbonation, the positive influence of porosity, which increases as carbonation progresses, becomes predominant over the increasing liquid-water saturation due to water production. After this initial rapid phase, the diffusion coefficient decreases because, during this period, the negative effect of liquid-water saturation becomes more influential than the increase in porosity caused by carbonation. Finally, after 15 min, the diffusion coefficient increases linearly because the positive effect of porosity and the negative effect of liquid-water saturation are balanced. However, porosity continues to dominate over liquid-water saturation due to the ongoing increase in the diffusion coefficient.

The study also explored the variation in porosity during carbonation, which was experimentally validated using a mercury intrusion porosimetry method. It was observed that the intragranular porosity (particle porosity) reduces directly to zero once the carbonation has started and that, on the contrary, the intergranular one (bed porosity) increases with carbonation. In this case, the bed porosity increases from 0.65 to 0.68 after 45 min of carbonation. This is very interesting because it is an opposite tendency in comparison to traditional materials like concrete, where carbonation typically reduces porosity [29,37,38]. This can be attributed to the fine nature of the material, where micropores are blocked as soon as calcium carbonate forms, and to the expansion of the solid volume related to the conversion of hydrated lime into less-dense calcium carbonate [20,28]. Although intra-granular porosity plays a minimal role due to particle size in this study, the model is robust enough to apply to scenarios with larger particles, where macroscale and microscale differentiation is crucial.

Moreover, the model accurately characterizes the variations in liquid-water saturation. First, it considers its positive influence on the kinetics of the reaction (no reaction in the absence of water), and second, it considers the negative effect for the diffusion of CO₂ when the system becomes saturated with water. However, the evaporation phenomena are not yet considered, leading to a small underestimation of the influence of the initial water-to-solid ratio in the process.

The experimental results have shown that, when hydrated lime is carbonated, the highest total carbon results are achieved with a CO₂ flow rate fixed at 200 mL·min⁻¹ and a water-to-solid ratio between 0.2 and 0.4. Regarding the CO₂ flow rate, this outcome is expected because the flushing of CO₂ in the reactor occurs more rapidly at higher flow rates.

The model has been validated through laboratory experiments, and its accuracy has been assessed using three different error-analysis methods. Initially, the relative errors between the experimental and the model results ranged from 3% to 27%, with higher relative errors observed when the initial water-to-solid ratio was high. However, regarding Figure 5, it is observed that all the points, with the exception of two, are within the range of

±20% of the difference, with the experimental results aligning with the goal established in the project.

Following this, the mean absolute percentage error (MAPE) was calculated. The model demonstrated good accuracy for lower initial water-to-solid ratios of 0.1 and 0.2, with MAPE values of 3% and 12%, respectively. However, for a ratio of 0.4, the MAPE increased to 19%, indicating reduced accuracy in this scenario. Further analysis involved calculating the root mean square error (RMSE). The model showed a strong correlation with the experimental results for ratios of 0.1 and 0.2, with RMSE values of 0.42 and 0.93, respectively. For the 0.4 ratio, the RMSE was 1.42, which is higher compared to the other two cases. In conclusion, the model exhibits good accuracy when applied to low initial water-to-solid ratios but shows reduced accuracy at higher ratios. This variance is due to the isothermal conditions assumed in the model. With a higher initial water content, more calcium hydroxide undergoes carbonation, leading to elevated temperatures and increased evaporation. The model does not account for evaporation, which results in higher simulated liquid-water saturation values compared to the actual measurements. Furthermore, it has been demonstrated that the mathematical model can be used to conduct sensitivity analyses to determine the optimal values of controllable process parameters.

Future work will aim to enhance the model by incorporating thermal balance to address heat release and evaporation during carbonation. The perspectives of our work are to expand the use of this tool to study the behavior of more complex materials, such as blended construction wastes, eventually leading to the optimal design of a large-scale mineralization process.

5. Conclusions

In summary, the presented model and experimental validation provide significant insights into the carbonation process, highlighting key factors such as porosity, liquid-water saturation, and CO₂ flow rate. These findings offer a foundation for future research and practical implementation, particularly in scaling up the carbonation process for industrial applications and its use to predict other materials' behaviors during the process of carbonation.

Author Contributions: Conceptualization, N.V.d.I.P., G.L. and D.T.; Methodology and validation, N.V.d.I.P., E.A., S.J. and S.M.; Software, N.V.d.I.P., G.L. and D.T.; Formal analysis, N.V.d.I.P., G.L. and D.T.; Investigation, Data curation, Writing, N.V.d.I.P., G.L. and D.T., Resources, E.A., S.J. and S.M., Data curation, N.V.d.I.P., G.L. and D.T.; Supervision, G.L. and D.T.; Project administration, E.A.; Funding acquisition, Walloon Region. All authors have read and agreed to the published version of the manuscript.

Funding: This research was financed by the Mineral Loop project, funded by the Walloon Region through the Greenwin Competitiveness Cluster (C8505).

Data Availability Statement: Data are contained within the article.

Conflicts of Interest: The authors declare no conflicts of interest.

References

1. Eurostat. Waste Statistics for EU. Available online: https://ec.europa.eu/eurostat/statistics-explained/index.php?title=Waste_statistics#Total_waste_generation (accessed on 8 April 2024).
2. Mudgal, S.; Hestin, M.; Trarieux, M.; Mimid, S. Service Contract on Management of Construction and Demolition Waste-SR1 European Commission (DG ENV). 2011. Available online: <https://circabc.europa.eu/ui/group/636f928d-2669-41d3-83db-093e90ca93a2/library/6d634cb1-0bd4-47e1-a4bb-eea94b350140/details> (accessed on 7 August 2024).
3. Internal Market, Industry, Entrepreneurship and SMEs; European Commission. Buildings and Construction. Available online: https://single-market-economy.ec.europa.eu/industry/sustainability/buildings-and-construction_en#:~:text=The%20construction%20sector%20is%20responsible,of%20total%20national%20GHG%20emissions (accessed on 10 July 2024).
4. Benhelal, E.; Zahedi, G.; Shamsaei, E.; Bahadori, A. Global strategies and potentials to curb CO₂ emissions in cement industry. *J. Clean. Prod.* **2013**, *51*, 142–161. [CrossRef]
5. Huijgen, W.J.J.; Witkamp, G.J.; Comans, R.N.J. Mechanisms of aqueous wollastonite carbonation as a possible CO₂ sequestration process. *Chem. Eng. Sci.* **2006**, *61*, 4242–4251. [CrossRef]

6. Werle, A.P.; Kulakowski, M.P.; De Souza Kazmierczak, C.; Alcântara, J.; Sentena, A. Carbonation in Concrete with Recycled Concrete Aggregates. In Proceedings of the DBMC International Conference on Durability of Building Materials and Components, Porto, Portugal, 12–15 April 2011.
7. Zhang, J.; Shi, C.; Li, Y.; Pan, X.; Poon, C.S.; Xie, Z. Influence of carbonated recycled concrete aggregate on properties of cement mortar. *Constr. Build. Mater.* **2015**, *98*, 1–7. [[CrossRef](#)]
8. Lange, L.C.; Hills, C.D.; Poole, A.B. The Effect of Accelerated Carbonation on the Properties of Cement-Solidified Waste Forms. *Waste Manag.* **1996**, *16*, 757–763. [[CrossRef](#)]
9. Andrade, C.; Sanjuán, M.Á. Updating carbon storage capacity of Spanish cements. *Sustainability* **2018**, *10*, 4806. [[CrossRef](#)]
10. Pade, C.; Guimaraes, M. The CO₂ uptake of concrete in a 100 year perspective. *Cem. Concr. Res.* **2007**, *37*, 1348–1356. [[CrossRef](#)]
11. Thiery, M.; Dangla, P.; Belin, P.; Habert, G.; Roussel, N. Carbonation kinetics of a bed of recycled concrete aggregates: A laboratory study on model materials. *Cem. Concr. Res.* **2013**, *46*, 50–65. [[CrossRef](#)]
12. La Peña, N.V.-D.; Grigoletto, S.; Toye, D.; Courard, L.; Léonard, G. CO₂ capture by mineral carbonation of construction and industrial wastes. In *Circular Economy Processes for CO₂ Capture and Utilization*, 1st ed.; Baena-Moreno, F.M., González-Arias, J., Ramírez-Reina, T., Pastor-Pérez, L., Eds.; Elsevier: Amsterdam, The Netherlands, 2023; Chapter 7.
13. Dowling, A.; O'Dwyer, J.; Adley, C.C. Lime in the limelight. *J. Clean. Prod.* **2015**, *92*, 13–22. [[CrossRef](#)]
14. Bing, L.; Ma, M.; Liu, L.; Wang, J.; Niu, L.; Xi, F. An investigation of the global uptake of CO₂ by lime from 1930 to 2020. *Earth Syst. Sci. Data* **2023**, *15*, 2431–2444. [[CrossRef](#)]
15. Erans, M.; Nabavi, S.A.; Manović, V. Carbonation of lime-based materials under ambient conditions for direct air capture. *J. Clean. Prod.* **2020**, *242*, 118330. [[CrossRef](#)]
16. Carmeuse. The Mineral LOOP Project. Available online: <https://www.carmeuse.com/eu-en/mineral-loop> (accessed on 22 August 2024).
17. Reich, L.; Yue, L.; Bader, R.; Lipiński, W. Towards solar thermochemical carbon dioxide capture via calcium oxide looping: A review. *Aerosol Air Qual. Res.* **2014**, *14*, 500–514. [[CrossRef](#)]
18. Thiery, M. *Modelling of Atmospheric Carbonation of Cement Based Materials Considering the Kinetic Effects and Modifications of the Microstructure and the Hydric State*; Ecole des Ponts ParisTech: Paris, France, 2005.
19. Morandau, A.; Thiéry, M.; Dangla, P. Investigation of the carbonation mechanism of CH and C-S-H in terms of kinetics, microstructure changes and moisture properties. *Cem. Concr. Res.* **2014**, *56*, 153–170. [[CrossRef](#)]
20. Cizer, Ö.; Rodriguez-Navarro, C.; Ruiz-Agudo, E.; Elsen, J.; Van Gemert, D.; Van Balen, K. Phase and morphology evolution of calcium carbonate precipitated by carbonation of hydrated lime. *J. Mater. Sci.* **2012**, *47*, 6151–6165. [[CrossRef](#)]
21. Rodriguez-Navarro, C.; Ilić, T.; Ruiz-Agudo, E.; Elert, K. Carbonation mechanisms and kinetics of lime-based binders: An overview. *Cem. Concr. Res.* **2023**, *173*, 107301. [[CrossRef](#)]
22. Gendron, F. Carbonatation des Matériaux Cimentaires: Étude de la Diffusion du CO₂. 2019. Available online: <https://theses.hal.science/tel-02520206> (accessed on 15 March 2024).
23. Šavija, B.; Luković, M. Carbonation of cement paste: Understanding, challenges, and opportunities. *Constr. Build. Mater.* **2016**, *117*, 285–301. [[CrossRef](#)]
24. Pham, S.T. Effects of Carbonation on the Microporosity and Macro Properties of Portland Cement Mortar CEM I. *J. Mater. Sci. Chem. Eng.* **2014**, *02*, 40–52. [[CrossRef](#)]
25. University of Liège. Multi-Scale Characterization of Porous Media-Mercury Intrusion. Available online: https://www.carpur.uliege.be/cms/c_14290809/en/carpur-mercury-intrusion (accessed on 22 August 2024).
26. LECCO EMPOWERING RESULTS 744 Series Carbon/Sulfur by Combustion. Available online: <https://www.leco.com/products/744-series/> (accessed on 9 August 2024).
27. Fang, F.; Li, Z.S.; Cai, N.S. CO₂ capture from flue gases using a fluidized bed reactor with limestone. *Korean J. Chem. Eng.* **2009**, *26*, 1414–1421. [[CrossRef](#)]
28. Gopinath, S.; Mehra, A. Carbon sequestration during steel production: Modelling the dynamics of aqueous carbonation of steel slag. *Chem. Eng. Res. Des.* **2016**, *115*, 173–181. [[CrossRef](#)]
29. Wu, B.; Ye, G. Development of porosity of cement paste blended with supplementary cementitious materials after carbonation. *Constr. Build. Mater.* **2017**, *145*, 52–61. [[CrossRef](#)]
30. Cui, H.; Tang, W.; Liu, W.; Dong, Z.; Xing, F. Experimental study on effects of CO₂ concentrations on concrete carbonation and diffusion mechanisms. *Constr. Build. Mater.* **2015**, *93*, 522–527. [[CrossRef](#)]
31. Wang, T.; Huang, H.; Hu, X.; Fang, M.; Luo, Z.; Guo, R. Accelerated mineral carbonation curing of cement paste for CO₂ sequestration and enhanced properties of blended calcium silicate. *Chem. Eng. J.* **2017**, *323*, 320–329. [[CrossRef](#)]
32. Schaefer, C.E.; Arands, R.R.; Van Der Sloot, H.A.; Kosson, D.S. Modeling of the gaseous diffusion coefficient through unsaturated soil systems. *J. Contam. Hydrol.* **1997**, *29*, 1–21. [[CrossRef](#)]
33. Partridge, G.P.; Lehman, D.M.; Huebner, R.S. Modeling the reduction of vapor phase emissions from surface soils due to soil matrix effects: Porosity/tortuosity concepts. *J. Air Waste Manag. Assoc.* **1999**, *49*, 412–423. [[CrossRef](#)]
34. Millington, R.J. Gas Diffusion in Porous Media. *Science* **1959**, *130*, 100–102. [[CrossRef](#)] [[PubMed](#)]
35. Tsimpanogiannis, I.N.; Moulτος, O.A.; Franco, L.F.M.; Spera, M.B.d.M.; Erdős, M.; Economou, I.G. Self-diffusion coefficient of bulk and confined water: A critical review of classical molecular simulation studies. *Mol. Simul.* **2019**, *45*, 425–453. [[CrossRef](#)]

36. Gallucci, E.; Scrivener, K. Crystallisation of calcium hydroxide in early age model and ordinary cementitious systems. *Cem. Concr. Res.* **2007**, *37*, 492–501. [[CrossRef](#)]
37. Bretti, G.; Ceseri, M.; Natalini, R.; Ciacchella, M.C.; Santarelli, M.L.; Tiracorrendo, G. A forecasting model for the porosity variation during the carbonation process. *GEM-Int. J. Geomath.* **2022**, *13*, 13. [[CrossRef](#)]
38. Muda, M.M.; Legese, A.M.; Urgessa, G.; Boja, T. Strength, Porosity and Permeability Properties of Porous Concrete Made from Recycled Concrete Aggregates. *Constr. Mater.* **2023**, *3*, 81–92. [[CrossRef](#)]

Disclaimer/Publisher’s Note: The statements, opinions and data contained in all publications are solely those of the individual author(s) and contributor(s) and not of MDPI and/or the editor(s). MDPI and/or the editor(s) disclaim responsibility for any injury to people or property resulting from any ideas, methods, instructions or products referred to in the content.